

On the origin of “patchy” energy conversion in electron diffusion regions

Cite as: Phys. Plasmas **29**, 082107 (2022); <https://doi.org/10.1063/5.0090275>

Submitted: 04 March 2022 • Accepted: 05 July 2022 • Published Online: 05 August 2022

 Kevin J. Genestreti,  Xiaocan Li,  Yi-Hsin Liu, et al.

COLLECTIONS

Paper published as part of the special topic on [Plasma Physics from the Magnetospheric Multiscale Mission](#)



View Online



Export Citation



CrossMark

ARTICLES YOU MAY BE INTERESTED IN

[Energetic electron scattering by kinetic Alfvén waves at strong magnetic field gradients of dipolarization front](#)

Phys. Plasmas **29**, 082901 (2022); <https://doi.org/10.1063/5.0096338>

[Electron heating in 2D: Combining Fermi–Ulam acceleration and magnetic-moment non-adiabaticity in a mirror-configuration plasma](#)

Phys. Plasmas **29**, 082106 (2022); <https://doi.org/10.1063/5.0097299>

[Resonant three-wave interactions with linear source/sink terms: Exploring the parameter space](#)

Phys. Plasmas **29**, 080701 (2022); <https://doi.org/10.1063/5.0098271>



Physics of Plasmas
Features in Plasma Physics Webinars

Register Today!

On the origin of “patchy” energy conversion in electron diffusion regions

Cite as: Phys. Plasmas **29**, 082107 (2022); doi: [10.1063/5.0090275](https://doi.org/10.1063/5.0090275)

Submitted: 4 March 2022 · Accepted: 5 July 2022 ·

Published Online: 5 August 2022



View Online



Export Citation



CrossMark

Kevin J. Genestreti,^{1,a)} Xiaocan Li,² Yi-Hsin Liu,² James L. Burch,³ Roy B. Torbert,^{1,4} Stephen A. Fuselier,^{3,5} Takuma Nakamura,^{6,7} Barbara L. Giles,⁸ Daniel J. Gershman,⁹ Robert E. Ergun,¹⁰ Christopher T. Russell,¹¹ and Robert J. Strangeway¹¹

AFFILIATIONS

¹Earth Oceans and Space, Southwest Research Institute, 8 College Rd., Durham, New Hampshire 03824, USA

²Department of Physics and Astronomy, Dartmouth College, Hanover, New Hampshire 03755, USA

³Space Science and Engineering, Southwest Research Institute, San Antonio, Texas 78238, USA

⁴Physics Department and Space Science Center, University of New Hampshire, Durham, New Hampshire 03824, USA

⁵Physics and Astronomy Department, University of Texas San Antonio, San Antonio, Texas 78249, USA

⁶Space Research Institute, Austrian Academy of Sciences, Graz 8042, Austria

⁷Institute of Physics, University of Graz, Graz 8010, Austria

⁸Goddard Space Flight Center, NASA, Greenbelt, Maryland 20771, USA

⁹NASA Goddard Space Flight Center, NASA, Greenbelt, Maryland 20771, USA

¹⁰Laboratory for Atmospheric and Space Physics, University of Colorado, Boulder, Colorado 80303, USA

¹¹Earth Planetary and Space Sciences, University of California Los Angeles, Los Angeles, California 90095, USA

Note: This paper is a part of the Special Collection: Plasma Physics from the Magnetospheric Multiscale Mission.

^{a)}Author to whom correspondence should be addressed: kevin.genestreti@swri.org

ABSTRACT

During magnetic reconnection, field lines interconnect in electron diffusion regions (EDRs). In some EDRs, the reconnection and energy conversion rates are controlled by a steady out-of-plane electric field. In other EDRs, the energy conversion rate $\vec{j} \cdot \vec{E}'$ is “patchy,” with electron-scale large-amplitude positive and negative peaks. We investigate 22 EDRs observed by NASA’s Magnetospheric Multiscale mission in a wide range of conditions to determine the cause of patchy $\vec{j} \cdot \vec{E}'$. The patchiness of the energy conversion is quantified and correlated with seven parameters describing various aspects of the asymptotic inflow regions that affect the structure, stability, and efficiency of reconnection. We find that (1) neither the guide field strength nor the asymmetries in the inflow ion pressure, electron pressure, nor number density are well correlated with the patchiness of the EDR energy conversion; (2) the out-of-plane axes of the 22 EDRs are typically fairly well aligned with the “preferred” axes, which bisect the time-averaged inflow magnetic fields and maximize the reconnection rate; and (3) the time-variability in the upstream magnetic field direction is best correlated with the patchiness of the EDR $\vec{j} \cdot \vec{E}'$. A 3D fully kinetic simulation of reconnection with a non-uniform inflow magnetic field is analyzed; the variation in the magnetic field generates secondary X-lines, which develop to maximize the reconnection rate for the time-varying inflow magnetic field. The results suggest that magnetopause reconnection, for which the inflow magnetic field direction is often highly variable, may commonly be patchy in space, at least at the electron scale.

Published under an exclusive license by AIP Publishing. <https://doi.org/10.1063/5.0090275>

I. INTRODUCTION

A. Background and motivation

Magnetic reconnection in plasmas plays an important role in converting magnetic energy to particle kinetic energy.^{1,2} At the

heart of magnetic reconnection is an electron diffusion region (EDR), where inflowing sheared magnetic fields merge, changing their connectivity.^{1,3,4} The reconnection electric field E_R cycles magnetic flux through the EDR, thereby mediating the local reconnection rate, maintaining the out-of-plane current density

J_M , and contributing to the energy conversion rate through $J_M E_R > 0$.⁵

NASA’s Magnetospheric Multiscale (MMS) mission investigates reconnection in Earth’s magnetosphere.⁶ In one EDR observed by MMS, a clear steady reconnection electric field, E_R , showed remarkable agreement with both the reconnection rate^{7–9} and electron energization rate.¹⁰ MMS has observed other EDRs with electron-scale peaks in the energy conversion rates that can exceed what is expected from typical values of E_R , in some cases by several orders of magnitude.^{11–17} These large-amplitude energy conversion rates often originate from spatially and/or temporally oscillatory electric fields such that $\vec{J} \cdot \vec{E}'$ displays both positive and negative values (where $\vec{E}' \equiv \vec{E} + \vec{v}_e \times \vec{B}$ is the electric field in the electron frame). We refer to such events as having “patchy” energy conversion rates.

Patchy EDR energy conversion has been observed by MMS more commonly at Earth’s magnetopause than in the magnetotail (e.g., analysis in Sec. III A)—though far fewer MMS magnetotail EDRs have been yet been identified. Magnetopause reconnection occurs between the highly variable shocked solar wind plasma and Earth’s magnetospheric plasma. Magnetotail reconnection occurs within the magnetosphere between similar plasmas. Whereas magnetopause reconnection often has pronounced asymmetries between the two inflow regions and may occur for a wide range of magnetic shear angles,¹⁸ magnetotail reconnection is often more symmetric with large magnetic shear angles.¹⁹ While a wide range of conditions of a reconnecting plasma may plausibly influence the structure of an EDR and its energy conversion rate, the seven parameters investigated here focus on conditions that typically differ for magnetopause and magnetotail reconnection.

B. Potential causes of patchy energy conversion

Asymmetries of upstream densities and magnetic field strengths can displace the inflow stagnation line and X-line.^{11,20} When the momenta of the two inflowing plasmas are imbalanced, a normal-directed current J_N crosses the X-line, which is unique to asymmetric reconnection.^{11,20–22} Heavier ions penetrate farther past the X-line than lighter electrons. Negative charge accumulation occurs as electrons converge on the electron inflow stagnation point, or S_e point for brevity. As these bunched electrons are deflected into the outflow, they meander back and forth across the low-density-side separatrix. The resulting oscillatory J_N and the strongly positive co-located E_N lead to

spatially oscillatory $J_N E_N$.^{12,23,24} Separation between the X and S_e lines may, therefore, lead to spatially patchy $\vec{J} \cdot \vec{E}'$ in EDRs.

Asymmetries of upstream densities and pressures can enable cross field density and pressure gradients at the X-line.²⁵ Lower-hybrid or electron drift instabilities may promote the growth of waves and turbulence around the EDR,^{26–32} which may alter the local energy conversion rate in and near the EDR.^{26,31} The most common form of drift wave found in/near MMS-observed asymmetric EDRs³² is a 3D corrugation-like surface wave that originates near the separatrices and ultimately results from an ion pressure gradient.^{28,29} Alternatively, the corrugation-like surface waves may be a branch of the lower-hybrid drift instability in which case they are expected to be driven by electron density or pressure gradients.^{30,32} Thus, the degree of asymmetry in the density, ion pressure, and/or electron pressure may lead to spatially and temporally patchy $\vec{J} \cdot \vec{E}'$.

During high-magnetic-shear reconnection, highly non-gyrotropic electron velocity distribution functions form as a result of cross field meandering motions^{7,11,33} and the energy conversion is primarily from perpendicular-to-the-magnetic-field currents and electric fields.³⁴ During low-shear reconnection, electrons are free to stream along a guide magnetic field^{16,17,35,36} and the energy conversion is primarily from parallel currents and electric fields.³⁴ These unstable velocity distribution functions in low and high magnetic shear EDRs have been shown to act as a free energy source for wave growth, which may modify the energy conversion rate within EDRs.^{13,37–39} Alternatively, the guide field may stabilize the EDR against the lower-hybrid drift instability.^{40,41}

Reconnection X-lines have preferred orientations, which optimize the reconnection rate.^{42,43} This optimum orientation, corresponding to the solid-line M direction in Fig. 1, bisects the upstream magnetic fields.⁴² If reconnection is forced to occur in an orientation that is not able to efficiently reconnect the inflowing magnetic energy (dashed M direction, Fig. 1), then secondary reconnection lines may develop along the optimal orientation.⁴³ This can occur when the reconnecting magnetic field is time-varying or has turbulent fluctuations, which will lead to flux pileup and flux rope generation in the outflow and modulations of the reconnection and flux transport rates.^{44,45} In 3D kinetic simulations, flux ropes often become entangled;^{46,47} it has been proposed that reconnection between entangled flux ropes may be the origin of patchy parallel electric fields

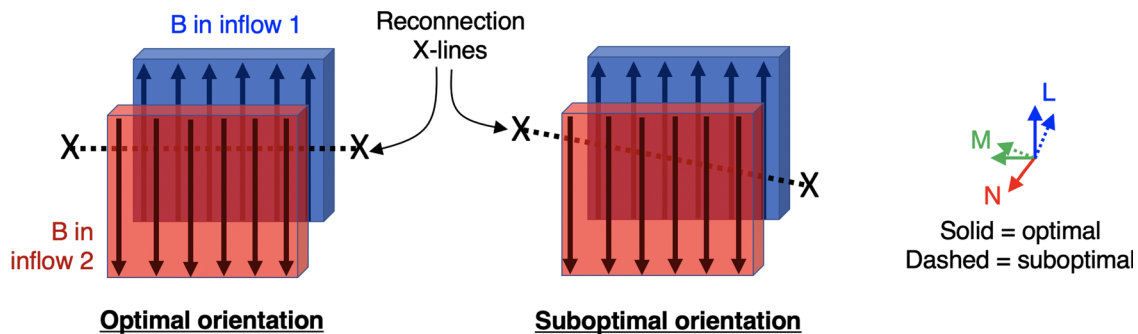


FIG. 1. Left: a reconnection X-line with the optimal orientation (solid-line M direction) that maximizes the upstream free magnetic energy and the reconnection rate. Right: reconnection with a suboptimal orientation (dashed-line M direction) reconnects the free magnetic energy inefficiently, leading to the growth of secondary reconnection lines that form with optimal orientations⁴³ (i.e., solid-line M direction).

observed by MMS.⁴⁸ Therefore, the time-varying upstream magnetic field could result in the patchy EDR $\vec{J} \cdot \vec{E}'$.

C. Outline of this study

To identify conditions in which patchy EDR energy conversion is most likely to be driven, we perform a multi-event study of 22 MMS-observed EDRs and correlate upstream parameters with the patchiness of the energy conversion. We find that the upstream parameter best-correlated with the patchiness of the energy conversion is the time variability of the upstream magnetic field direction. We then perform a large, 3D, and fully kinetic particle-in-cell (PIC) simulation of reconnection with a time-varying upstream field. We find that the current sheet develops secondary tearing lines that have orientations that maximize the reconnection rate of varying inflow fields.

Parameter definitions, methodologies for their identification, and a description of the relevant capabilities of MMS are found in Sec. II. In Sec. III A, we present results of the multi-event study, finding that the strongest correlation is between the patchiness of the EDR energy conversion rate and time variability of the upstream magnetic field direction. In Sec. III B, we analyze a three-dimensional fully kinetic particle-in-cell (PIC) simulation of reconnection with an unsteady upstream magnetic field. Finally, in Sec. IV, we summarize and interpret these results.

II. METHODOLOGY AND MMS DATASET

A. Overview of methodology

We seek to understand whether one or more of several of the following descriptors of the upstream plasma conditions, enumerated below, may play a predominant role in controlling the patchiness of the EDR energy conversion rate $\sigma_{\vec{J} \cdot \vec{E}'}$.

1. Distance along the normal direction between the X and S_e lines (δ_{XSe}) normalized by the thickness of the EDR $2\delta_e$, which is estimated as

$$\delta_{XSe}/2\delta_e = \frac{n_1 B_{L2}^2 - n_2 B_{L1}^2}{(B_{L1} + B_{L2})(n_1 B_{L2} + n_2 B_{L1})}, \quad (1)$$

where n is the number density, B_L is the reconnecting component of the magnetic field, and subscripts 1 and 2 indicate that the parameter is associated with one or the other inflow region.¹⁵

2. Ion thermal pressure asymmetry $(\langle P_{i1} \rangle - \langle P_{i2} \rangle)/P_{i0}$, where subscripts 1 and 2 denote the asymptotic pressures in the two inflow regions and the normalization parameter P_{i0} is hybrid asymptotic scalar ion pressure, assumed to follow

$$P_{i0} = n_0 T_{i0} = \left(\frac{n_1 B_2 + n_2 B_1}{B_1 + B_2} \right) \left(\frac{n_1 T_{i1} B_2 + n_2 T_{i2} B_1}{n_1 B_1 + n_2 B_2} \right), \quad (2)$$

based on previously derived expressions for the hybrid asymptotic number density²⁰ and temperature.¹⁵

3. Electron thermal pressure asymmetry $(\langle P_{e1} \rangle - \langle P_{e2} \rangle)/P_{e0}$, where P_{e0} follows the form of Eq. (2), where angular brackets indicate time averages.
4. Number density asymmetry $(\langle n_1 \rangle - \langle n_2 \rangle)/n_0$, where n_0 is given by the left-most parenthetical term in Eq. (2).
5. Normalized guide magnetic field strength B_G/B_{L0} , B_{L0} is the hybrid reconnecting magnetic field component, which follows²⁰

$$B_{L0} = \frac{2B_{L1}B_{L2}}{B_{L1} + B_{L2}} \quad (3)$$

and the hybrid asymptotic guide field B_G is assumed to follow the same form.

6. Angle between the actual and optimal (M_{opt}) X-line orientations in the L - M plane, where M_{opt} bisects the time-averaged inflow magnetic fields.⁴²
7. Angular variability in the upstream magnetic fields $\delta\theta = \langle \text{acos}(\hat{B} \cdot \langle \hat{B} \rangle) \rangle$.

The “patchiness” of the EDR energy conversion rate $\sigma_{\vec{J} \cdot \vec{E}'}$ is quantified as the deviation between the observed $\vec{J} \cdot \vec{E}'$ and the energy conversion rate expected from a steady reconnection electric field (i.e., as the standard deviation of the difference of the red and black curves in Fig. 2 normalized by the maximum value of the red curve), i.e.,

$$\sigma_{\vec{J} \cdot \vec{E}'} = \frac{\sqrt{\langle (\vec{J} \cdot \vec{E}' - J_M E_R)^2 \rangle - \langle \vec{J} \cdot \vec{E}' - J_M E_R \rangle^2}}{\max(J_M E_R)}, \quad (4)$$

where $\vec{E}' \equiv \vec{E} + \vec{v}_e \times \vec{B}$ is the electric field in the electron rest frame, i.e., the non-ideal electric field, and the normalization quantity is the maximum value of $J_M E_R$ in the EDR. E_R is a constant value determined as $E_R = R(V_{A0} B_0)$, where R is the normalized reconnection rate and the theoretical maximum $R \simeq 0.2$ value^{49,50} is assumed, V_{A0} is the hybrid asymptotic upstream ion Alfvén speed, and B_0 is the hybrid asymptotic upstream reconnecting magnetic field B_L . Note that the exact choice of $R = 0.2$ does not substantially affect the results of the study, as is demonstrated in Appendix B. With the exception of E_R , all other parameters in Eq. (4) are evaluated in the EDR. Figure 2(a) shows an extremely laminar EDR energy conversion case, while Fig. 2(b) shows an extremely patchy event.

If patchy EDR energy conversion results from charge accumulation at the S_e line, then large-amplitude and spatially oscillatory $J_N E'_N$ should contribute predominantly to the overall product $\vec{J} \cdot \vec{E}'$. We also define and calculate separate patchiness terms for $J_L E'_L$, $J_M E'_M$, and $J_N E'_N$.

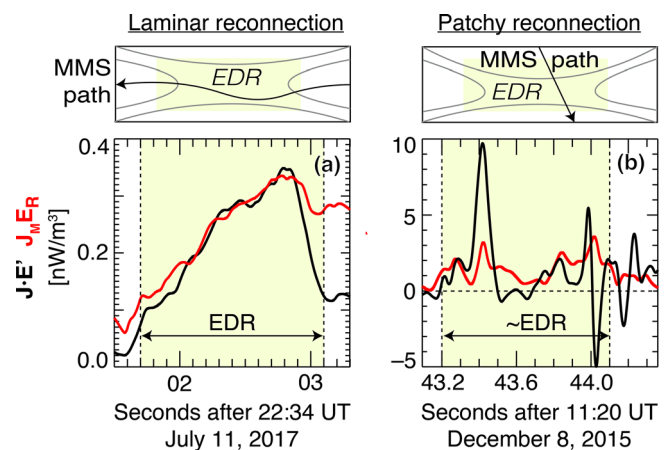


FIG. 2. A comparison of the observed non-ideal energy conversion rate $\vec{J} \cdot \vec{E}'$ and the rate expected based on a uniform and constant reconnection electric field $J_M E_R$. Two events are shown, which were identified in Earth’s magnetotail⁵¹ (left) and at the magnetopause³⁶ (right).

$$\sigma_{J_i \cdot E_i} = \frac{\sqrt{\langle (J_i E_i' - \delta_{iM} J_M E_R)^2 \rangle - \langle (J_i E_i' - \delta_{iM} J_M E_R) \rangle^2}}{\max(J_M E_R)}, \quad (5)$$

where i is L , M , or N and $\delta_{iM} = 1$ for $i = M$ and zero otherwise.

B. MMS dataset

MMS consists of four identically equipped spacecraft that, during the periods studied here, flew in an electron-scale tetrahedral formation.^{6,52} MMS science data are available in two principal modes, burst, and survey, which describe the resolution of the data returned to ground. High-resolution burst-mode data are typically only available during current sheet crossings and are required for analyzing EDRs. Lower-resolution survey mode data are used when analyzing the asymptotic inflow regions.

The fast plasma investigation obtains 3D velocity distribution functions and moments of ions and electrons once per 150 and 30-ms, respectively, in burst mode (4.5-s cadences for both species in survey mode).⁵³ For magnetopause EDRs, mass-per-charge-separated ion composition data from the hot plasma composition analyzer⁵⁴ are used to help distinguish the magnetosheath, magnetosphere, and mixed boundary layer plasmas. Comparatively high He^{++} and negligible O^+ concentrations are expected in the asymptotic upstream magnetosheath, while the opposite is expected in the magnetosphere inflow region. 3D electric and magnetic field measurements are obtained by the electric field double probes^{55,56} and flux gate magnetometers,⁵⁷ respectively. Burst-mode electric field data are available at 8192 Hz. Survey-mode magnetometer data are available at 8 Hz. The particle moments from the fast plasma investigation are used to calculate current densities uniquely at each of the four spacecraft.⁵⁸ $\vec{J} \cdot \vec{E}'$ is also calculated uniquely at each spacecraft and is smoothed to remove sub- d_e -scale oscillations.

C. Analysis methods and event selection criteria

First we identify EDR events. Throughout this paper, EDR refers to the “central EDR,” which is distinguished from the extended electron jet region often referred to as the “outer EDR.”^{59,60} Generally speaking, the central EDR is where field lines merge.^{4,67,61} Even during laminar reconnection, $\vec{J} \cdot \vec{E}' < 0$ is expected⁶¹ and observed in the outer EDR,⁶² as super-Alfvénic electron jet braking causes the electron-frame out-of-plane electric field component (E_M') to be anti-aligned with the out-of-plane current;^{9,63} since the energy conversion rate is, therefore, not controlled by $J_M E_R$ in the outer EDR, such intervals are excluded from this study. Central EDR intervals were identified by eye on a case-by-case basis using (1) large $J_M \gtrsim J_L$, (2) significant electron pressure non-gyrotropy, and (3) predominantly positive $\vec{J} \cdot \vec{E}'$. We started with 36 EDR events, 34 of which were identified at the dayside magnetopause^{11,14,17,24,27,36,51,64–68} and 2 in the magnetotail.^{7,69}

Next, we require that MMS observed both asymptotic inflow regions for several minutes. The trajectory MMS that takes through an EDR depends almost entirely on the time-dependent motion of the EDR, which varies from event to event. In some cases, MMS does not fully cross the EDR into one inflow region; these events are discarded, leaving 27 EDRs. Three events for which plasma parameters during an inflow interval could not clearly be associated with the EDR interval

(e.g., when large rotations in the upstream magnetic field were observed during the crossing) were discarded, leaving 24 EDRs.

Average LMN coordinates were determined for these 24 EDRs. Here, average specifies that a single coordinate system is used to define an EDR interval, whereas the axes may vary during the crossing.⁷⁰ The maximum directional derivative of \vec{B} (MDD-B) technique⁷¹ was used to identify the EDR current sheet normal N . For some events, MDD-B did not find a stable normal direction; in these cases, maximum variance of the electric field^{72,73} (MVA-E) was used to identify N . Maximum variance of the magnetic field⁷⁴ (MVA-B) was then used to determine a direction L^* . M was then evaluated as $N \times L^* / |N \times L^*|$ and $L = M \times N$. Similar hybrid techniques for finding LMN coordinates have been used previously.^{8,70} Two events were discarded because EDR coordinates could not be confidently established, leaving 22 total EDR events for this study (20 magnetopause and 2 magnetotail events).

We use Spearman’s ρ coefficient to evaluate the strength of the correlations between the patchiness of the energy conversion in our 22 EDRs with the seven parameters enumerated in the list of Sec. II A. ρ is a non-parametric measure of the strength with which two variables are associated.⁷⁵ This approach was chosen because (1) the magnitude of ρ is not strongly influenced by outlying data points and (2) we do not have to assume any particular functional form describing the relationships between the patchiness and the seven parameters; rather, only a monotonic relationship is assumed. We refer to correlations with $|\rho| \leq 1/3$ as weak, $1/3 \leq |\rho| \leq 2/3$ as moderate, and $|\rho| \geq 2/3$ as strong. We also evaluate a confidence interval for each correlation, i.e., the probability that a non-zero correlation is not the result of random chance, which is based on the sample size (22 EDRs) and the strength of the correlation ($= 1 - \rho\sqrt{2}$). We adopt a “95% rule,” meaning that only correlations with $\geq 95\%$ confidence (2σ) are deemed significant.

III. RESULTS

A. Multi-event study

Figures 3(a)–3(e) show the patchiness of the 22 EDRs vs the first five parameters in the enumerated list in Sec. II A. As noted in Sec. I, the 20 magnetopause EDRs (orange symbols) are typically more patchy than the 2 magnetotail EDRs (purple symbols). Of the five parameters shown in Figs. 3(a)–3(e), the separation between the X and S_e lines [Fig. 3(a)], as defined in Eq. (1), is the only parameter strongly and significantly correlated with the patchiness of the energy conversion. A note of caution is required, however, regarding the clustering of data points in the parameter space of Fig. 3(a). Since we do not have enough EDRs to control for all parameters simultaneously, it is not possible to discern whether the separation of magnetotail [two bottom/left-most data points in Fig. 3(a)] and magnetosheath [20 right-most data points in Fig. 3(a)]. EDRs are due to unique aspects of reconnection caused by X and S_e line separations or due to other differences between the magnetopause and magnetosheath current sheets. However, when the two outlying magnetotail data points are excluded, the correlation coefficient and confidence drop only slightly to 0.61 and 99.2%, respectively, meaning that the correlation becomes moderate but remains significant. Figure 3(b) shows the component-specific patchiness parameter of Eq. (5). If charge accumulation at the S_e line was the predominant cause of patchy energy conversion, then the energy

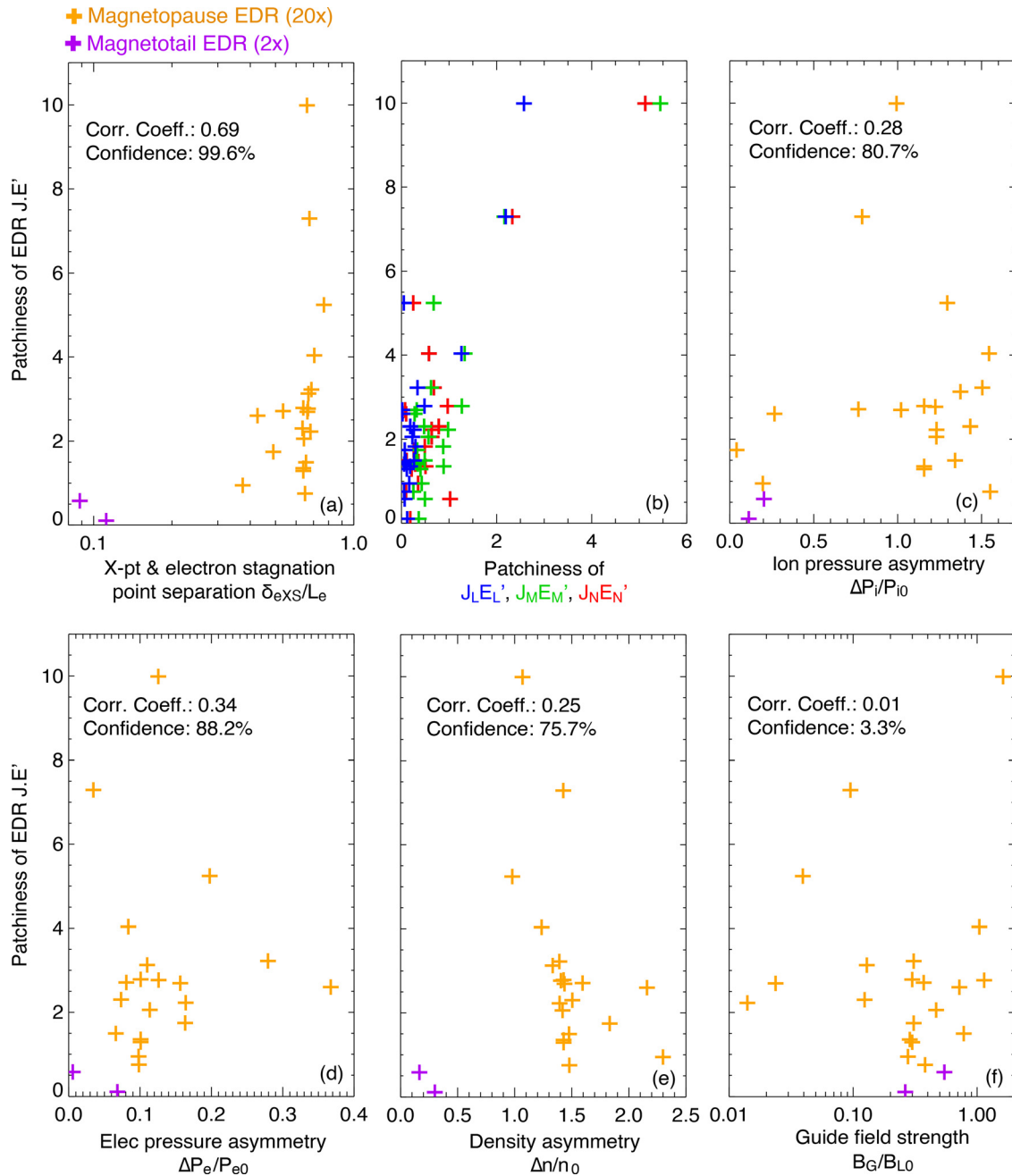


FIG. 3. Vertical axes are $\sigma_{J \cdot E'}$ defined in Eq. (4) for 22 EDRs. Horizontal axes are the normalized: (a) separation between the X and electron stagnation (S_e) lines, a derived quantity based on the inflow magnetic field and density asymmetries, (b) the patchiness of $J_L E_L'$ (blue), $J_M E_M'$ (green), and $J_N E_N'$ (red), as defined in Eq. (5), (c) scalar ion thermal pressure asymmetry, (d) scalar electron thermal pressure asymmetry, (e) density asymmetry, and (f) guide field strength; the definitions of which are found in the numbered list in Sec. II A. (a) and (c)–(f): Spearman correlation coefficients and their confidence values are in the upper left of each panel, magnetopause EDRs are colored orange, and magnetotail EDRs are purple.

conversion rates of patchier events are expected to be dominated by $J_N E_N'$. However, there is no clear dominance of the patchiness of $J_L E_L'$ (blue), $J_M E_M'$ (green), and $J_N E_N'$ (red) to the overall patchiness of $\vec{J} \cdot \vec{E}'$.

Weak correlations were found between the patchiness of the energy conversion and the ion [Fig. 3(c)] and electron [Fig. 3(d)] thermal pressure asymmetries, the density asymmetry [Fig. 3(e)], and the guide field strength [Fig. 3(f)]; all correlations were all below our 95%

confidence threshold for significance. Observations and simulations suggest that these parameters may play a role in modulate the energy conversion rate at or very near the EDR, at least in some limiting circumstances. Since we are unable to control for all parameters simultaneously, the results of Fig. 3 may only be interpreted as evidence that these parameters do not exert a singular or predominant influence on the patchiness of the EDR energy conversion, over the parameters' ranges typically found in the magnetosphere.

The final two parameters from Sec. II A are shown in Figs. 4(a) and 4(b): The angle between the actual EDR M and optimum M_{opt} directions and the angular variability of the upstream magnetic field, respectively. Errors in the EDR coordinate axes determined with the hybrid MDD-B/MVA technique may be $\sim 4^\circ$ -to- 10° based on previous MMS case analyses;^{8,70} analysis of our 3D simulation run (Sec. III B) with this hybrid method yielded an error of $\sim 5^\circ$ in the M direction. We find that most of the EDRs are separated from the optimum M_{opt} direction by angles less than our assumed 10° of uncertainty.

The parameter most strongly and significantly correlated with $\sigma_{J,E}$ is the time variability of the upstream magnetic field direction [Fig. 4(b)]. This correlation may indicate that, while the EDR may be fairly well aligned with the time-averaged optimum M_{opt} direction, time variations in M_{opt} may also lead to secondary tearing growth. This result is in good agreement with recent two-dimensional particle-in-cell simulations⁴⁴ of reconnection with fluctuating magnetic fields. In Sec. III B, we investigate this result further by analyzing a three-dimensional simulation of reconnection with a non-uniform inflow magnetic field.

B. Simulation of reconnection with varying inflow conditions

A three-dimensional fully kinetic simulation was performed to investigate the behavior of reconnection under non-uniform inflow conditions. The simulation was run using the electromagnetic particle-in-cell code VPIC.⁷⁶ The initial magnetic field profile of the primary asymmetric current sheet was taken from a previous work;⁴³ however, a tangential discontinuity (TD) was added in the upstream magnetosheath [see Fig. 7(b)]. The TD convects with the inflow toward the X-line, meaning the spatial variations in the inflow field translate to time-varying boundary conditions for the diffusion region. The upstream TD was an ion-scale rotation of the inflow magnetic field by 45° , which was chosen to loosely match the largest variations in the upstream field direction for the event of Fig. 2(b). We stress, however, that this is not a simulation of an MMS event, and variations in the upstream magnetic field only occur at the TD. To reduce turbulence resulting from periodic conditions at the M boundaries, the simulation box was oriented such that the optimal M_{opt} direction of the primary reconnecting current sheet was aligned with the simulation M coordinate.⁴³ A full description of the 3D simulation setup is provided in Appendix A 1.

We limit our investigation to a single time of the simulation, $t = 128/\Omega_{ci}$ (where Ω_{ci} is the ion cyclotron period), which is roughly $50\Omega_{ci}$ after the TD convected into the diffusion region. At this time, strong $\vec{J} \cdot \vec{E}'$ resulting from the initial conditions was no longer apparent. At $t = 128/\Omega_{ci}$, some readily identifiable impacts of the time-varying inflow appear in the simulation.

Figures 5(a) and 5(b) show a cut through the L - M plane at $N/d_e = 1$, the approximate location of the primary X-line. In the

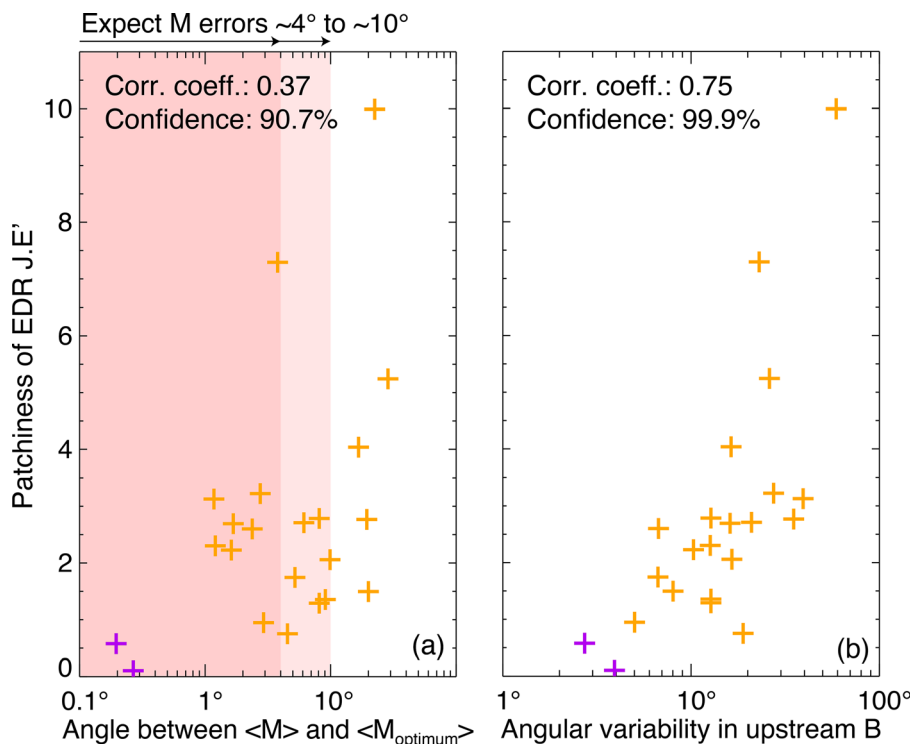


FIG. 4. Vertical axes are $\sigma_{J,E}$ defined in Eq. (1) for 22 EDRs. Horizontal axes are: (a) the angular difference in the L - M plane between the EDR M direction and the optimum M direction, which bisects the time-averaged upstream magnetic fields and (b) the angular variability of the upstream magnetic field direction. Spearman correlation coefficients and confidence values are in the upper left of each panel. Magnetopause EDRs are colored orange, and magnetotail EDRs are purple.

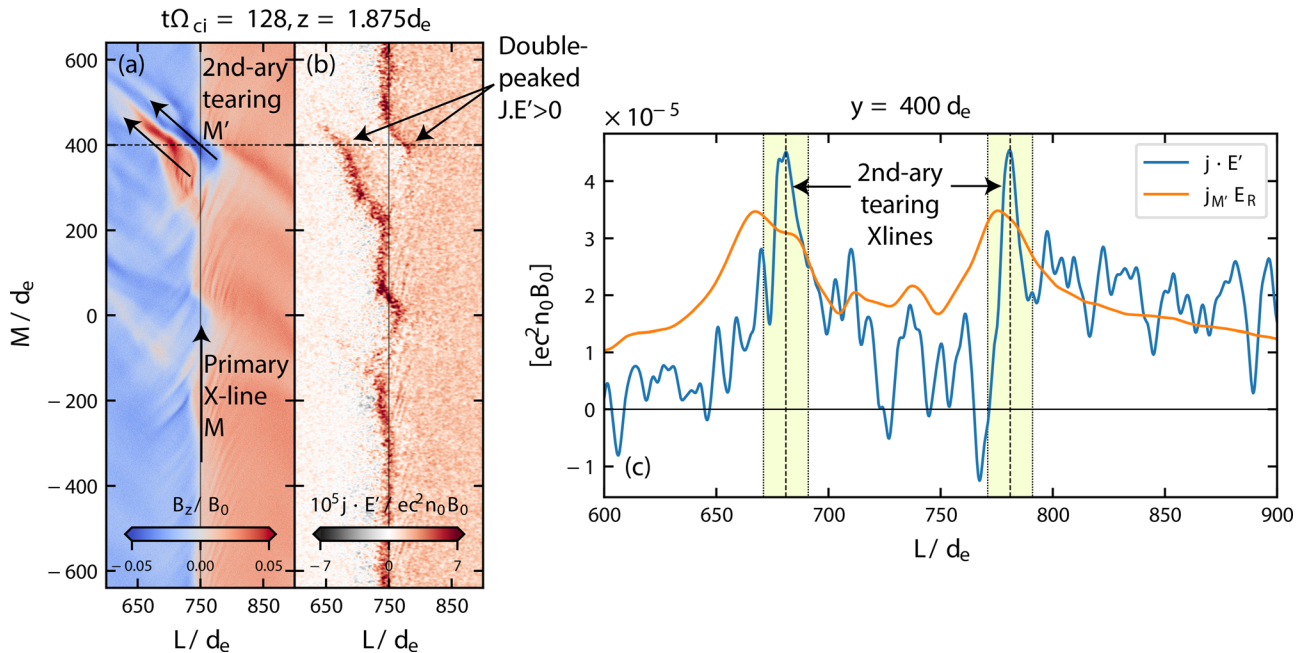


FIG. 5. Cuts of the 3D run showing the (a) reconnected component of the magnetic field, (b) electron-frame energy conversion rate in the simulation L - M plane, and (c) $\vec{j} \cdot \vec{E}'$ (blue) and $J_{M'} E_R$ (orange), where M' is the local M direction for the secondary X-lines [shown in (a)]. The shaded boxes indicate the region within $\pm 10 d_e$ of the X-lines.

L - M plane, reconnection lines are identified as dividing lines that separate oppositely directed B_N . Secondary tearing lines, shown in Fig. 5(a), are likely a result of the TD impact. The axes of the secondary tearing lines M' are tilted by roughly 45° relative to the primary X-line M , which is consistent with the expected optimal M direction (along the line bisecting the upstream fields^{42,43}) after the 45° rotation of the upstream \vec{B} associated with the TD. Persistent features associated with the primary X-line, which was oriented in the optimal direction under the initial upstream conditions, appear simultaneously with the secondary tearing modes.

Figure 5(c) shows $\vec{j} \cdot \vec{E}'$ and $J_{M'} E_R$ along a 1D cut through the secondary tearing lines, comparable in layout to Fig. 2. Shaded boxes in Fig. 5(c) indicate the region within $\pm 10 d_e$ of the X-line, corresponding very roughly to the EDR length in the outflow direction.⁷⁷ The reconnection rate was slow at this late stage of the simulation, with $R = 0.03$ based on the normalized inflow speeds (not pictured). The slow rate may be due to the inflow magnetic flux relative being depleted by $\sim 25\%$ relative to its initial value (not pictured). When the normalized rate of 0.03 is used to calculate E_R , we obtain patchiness parameters $\sigma_{J \cdot E'}$ of 0.28 and 0.38 for the X-lines at $L = 681 d_e$ and $781 d_e$, respectively. When a reconnection rate of 0.2 is used, $J_{M'} E_R$ exceeds $\vec{j} \cdot \vec{E}'$ by such a wide margin that were this observed by MMS, it would likely be excluded from our event list. The values of $\sigma_{J \cdot E'}$ are very low relative to MMS events, yet so is the angular variability in the upstream magnetic field (1.9°), making it consistent with the correlation of Fig. 4(b). It is likely that the reconnection at this late stage has already reached a steady state under the steady post-TD impact inflow fields and, hence, the good agreement between $\sigma_{J \cdot E'}$ and $J_{M'} E_R$.

A 2.5-dimensional fully kinetic simulation was performed with steady upstream conditions (i.e., there is no upstream TD in the 2.5D

run) to demonstrate that small $\sigma_{J \cdot E'}$ is found for reconnection at a steady state. The initial conditions of the 2.5D run match those of the 3D run after the TD impact (see Appendix A 2). Lower noise levels are present in the 2.5D run, meaning that $\sigma_{J \cdot E'}$ can be determined at any time and is determined here while the reconnection rate was order 0.1. Results from the 2.5D run are shown in Fig. 6. Cuts in Fig. 6 are shown at time $t = 74/\Omega_{ci}$, at which point no secondary X-lines were present. Near the X-line, in the shaded region of Fig. 6(c), $\vec{j} \cdot \vec{E}'$ and $J_{M'} E_R$ agree very well, indicating that the 2.5D steady simulation did not have patchy energy conversion. When normalized reconnection rates of $R = 0.1$ [Fig. 6(c)] and $R = 0.2$ (not pictured) are used, the patchiness parameter $\sigma_{J \cdot E'}$ is 0.36 and 0.16, respectively. Comparisons with MMS events [e.g., Fig. 3(a)] reveal that this steady simulation has a $\sigma_{J \cdot E'}$ similar to the least patchy EDR MMS has observed: the event shown in Fig. 2(a).

IV. SUMMARY, INTERPRETATION OF RESULTS, AND FUTURE WORK

The overarching goal of this study was to determine the origin of patchy non-ideal energy conversion rates $\vec{j} \cdot \vec{E}'$ commonly found in MMS-observed electron diffusion regions (EDRs). We examined 36 EDRs, finding 22 that were suitable for a multi-event study. The patchiness of the energy conversion rate was quantified by $\sigma_{J \cdot E'}$, as defined in Eq. (4), which is the difference between the MMS-observed energy conversion rate and the rate expected from a uniform, steady reconnection electric field with a normalized strength of 0.2 (though the choice of 0.2 does not substantially affect the results, as demonstrated in Fig. S11). The patchiness of the energy conversion was then correlated with seven parameters describing the geometry of the diffusion region and its upstream conditions: the (1) separation between the X

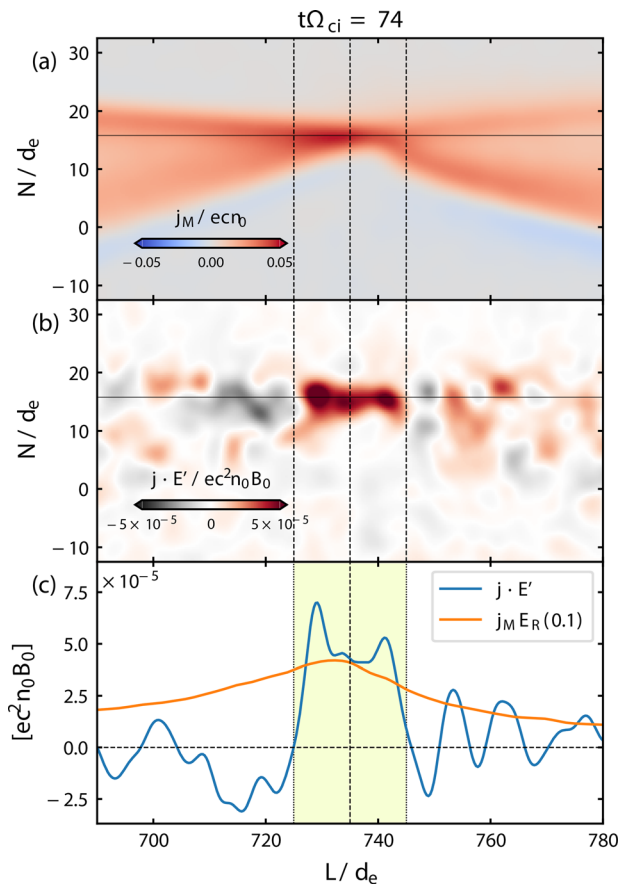


FIG. 6. Cuts of the 2.5D run showing the (a) out-of-plane current J_M and (b) non-ideal energy conversion rate $\vec{J} \cdot \vec{E}'$ in the L - N plane and (c) a cut along the outflow direction L of $\vec{J} \cdot \vec{E}'$ (blue) and $J_M E_R$ (orange), where $R = 0.1$ is used to calculate E_R . The shaded box indicates the region within $\delta L = \pm 10d_e$ of the X-line.

and electron stagnation (S_e) lines, a function of the magnetic field and density asymmetry, (2) ion scalar pressure asymmetry, (3) electron scalar pressure, (4) density asymmetry, (5) guide field strength, (6) the angle between the average EDR and optimum M directions, the latter being the line bisecting the time-averaged upstream magnetic fields, and (7) the time variability of the upstream field.

The following are the principal findings from the multi-event study:

1. The patchiness of the energy conversion rates in our EDR events is not correlated with the density asymmetry, ion, and electron pressure asymmetries, nor the guide field strength.
2. A strong and significant correlation is observed between the patchiness of the EDR energy conversion and the separation between the X and S_e lines, which is a function of the magnetic field and density asymmetry. There is no clear dominance of $J_L E'_L$, $J_M E'_M$, or $J_N E'_N$ in EDRs with patchy energy conversion.
3. The majority of EDRs have an average M direction within (10°) uncertainty bars of being aligned with the optimum direction, which bisects the time-averaged upstream magnetic fields and maximizes the reconnection rate.

4. The best correlation is observed between the patchiness of the EDR energy conversion and the time variability of the upstream magnetic field direction.

A three-dimensional particle-in-cell (PIC) simulation was performed to investigate the behavior of reconnection with non-uniform inflow conditions. Reconnection began along a primary X-line, which had an optimum orientation that bisected the initial upstream field, thereby maximizing the initial reconnection rate. After a tangential discontinuity impacted the diffusion region and the immediately upstream magnetic field rotated by 45° secondary tearing lines developed, which radiate from the primary X-line at an angle consistent with the change in the magnetic shear (by 45°). Due to high noise levels, which may have been due in part to an initial state of disequilibrium, we were not able to quantify the patchiness of the energy conversion during the TD impact in the simulation studied here. Analysis of the 3D run long after the TD impact reveals that reconnection had already reached a steady state, and $\sigma_{J \cdot E'}$ was very small, consistent with the low variability in the upstream magnetic field and the observationally derived correlation of Fig. 4(b).

We interpret the findings in the following way: of the sources studied here, the predominant source of patchiness in the EDR energy conversion rate is the time variability of the inflowing magnetic field directions. The causal relationship may be due to the formation of secondary tearing lines, which develop from a primary tearing line in unsteady inflow conditions, as was seen in the simulation. Whereas the direction of the primary reconnection line seems to be (at least, most commonly) set by the direction that bisects the time-averaged upstream fields, the growth of secondary tearing lines may be the mechanism that maximizes the reconnection rate under time-varying inflow fields. This is just one possible interpretation, since no clear enhancement in $\vec{J} \cdot \vec{E}'$ was observed at the simulated secondary tearing lines. It is possible the single clean variation in the simulated magnetic field was not complex enough in its structure to lead to entangled flux rope formation^{46–48} and discernibly patchy $\vec{J} \cdot \vec{E}'$. Additionally, it is likely that, at the late stage of the 3D simulation considered here, the reconnection had already reached a steady state and, therefore, had very good agreement between the observed energy conversion rate and the rate expected from a steady reconnection electric field.

This interpretation is comparable to findings from previous works, which studied in two-dimensional PIC simulations and found that the growth of secondary tearing lines and modulations in the reconnection rate result from time-varying inflow magnetic field configurations.^{44,45} In comparison with the aforementioned two-dimensional pictures, we suggest that the secondary tearing lines may form with oblique (3D) geometries such that the reconnection rate is maximized for the time-varying field. Our interpretation and findings are also comparable with earlier MMS-based investigations. These studies suggested that patchiness in the reconnection rate may lead to the formation of tangled flux ropes, which, in turn, may reconnect with one another and generate patchy and large-amplitude electric fields.⁴⁸ Additionally, our interpretation may be consistent with recent results, suggesting that large enhancements of $\vec{J} \cdot \vec{E}'$ are associated with secondary “electron-only” reconnection lines.⁷⁸

Further simulation work is needed to develop a quantitative relationship between unsteady inflow magnetic fields and patchy reconnection. In addition to existing studies of two-dimensional simulations, three-dimensional simulations should be conducted to

determine whether entanglement and reconnection of secondary flux ropes lead to enhanced energy conversion rates.

One question that cannot be answered at present is whether or not patchy electron-scale reconnection has a discernible impact on reconnection at larger scales. It has recently been suggested that at/above ion scales, reconnection at Earth's magnetopause appears to have a continuous global-scale structure.⁷⁹ Reconciling the patchiness of reconnection at electron-scales with the apparent continuous and quasi-two-dimensional nature of reconnection at much larger scales may be possible in the near future as in its current extended mission, the inter-spacecraft separations will be increased such that MMS will be able to resolve electron and ion-scales simultaneously.

ACKNOWLEDGMENTS

We acknowledge the contributions made by many MMS team members to the success of the mission and the accessibility and high quality of the MMS data. This study has used several routines from the Space Physics Environment Data Analysis System⁸⁰ and has benefited from conversations with Dr. Michael Hesse, Dr. Richard Denton, Dr. Paul Cassak, and Dr. Dominic Payne. The simulation is performed on Frontera at Texas Advanced Computer Center (TACC). K.J.G. is supported by NASA Grant No. 80NSSC20K0848. X.L. and Y.L. are supported by MMS Grant No. 80NSSC18K0289.

AUTHOR DECLARATIONS

Conflict of Interest

The authors have no conflicts to disclose.

Author Contributions

Kevin J. Genestreti: Conceptualization (lead); Data curation (lead); Formal analysis (lead); Funding acquisition (lead); Investigation (lead); Methodology (lead); Project administration (lead); Resources (lead); Software (equal); Supervision (equal); Validation (equal); Visualization (equal); Writing – original draft (lead); Writing – review and editing (lead). **Robert E. Ergun:** Data curation (supporting); Supervision (supporting). **Christopher Thomas Russell:** Data curation (supporting); Supervision (supporting); Writing – review and editing (supporting). **Robert J. Strangeway:** Data curation (supporting); Supervision (supporting). **Xiaocan Li:** Data curation (supporting); Formal analysis (supporting); Investigation (supporting); Software (equal); Visualization (equal); Writing – original draft (supporting); Writing – review and editing (supporting). **Yi-Hsin Liu:** Conceptualization (equal); Data curation (equal); Formal analysis (supporting); Investigation (supporting); Methodology (supporting); Resources (equal); Software (supporting); Supervision (equal); Writing – original draft (supporting); Writing – review and editing (supporting). **James Leo Burch:** Data curation (supporting); Investigation (supporting); Methodology (supporting); Resources (supporting); Software (supporting); Supervision (supporting); Writing – review and editing (supporting). **Roy Torbert:** Data curation (supporting); Funding acquisition (supporting); Investigation (supporting); Supervision (supporting). **Stephen Fuselier:** Data curation (supporting); Investigation (supporting); Supervision (supporting); Writing – review and editing (supporting). **Takuma Nakamura:** Investigation

(supporting); Writing – review and editing (supporting). **Barbara L. Giles:** Data curation (equal); Project administration (supporting); Supervision (supporting); Writing – review and editing (supporting). **Daniel J. Gershman:** Data curation (supporting); Supervision (supporting); Writing – review and editing (supporting).

DATA AVAILABILITY

The data that support the findings of this study are openly available at <https://lasp.colorado.edu/mms/sdc/public/>, Ref. 81. The simulation is available upon request to Xiaocan Li (Xiaocan.Li@dartmouth.edu).

APPENDIX A: SIMULATION SET-UP AND ANALYSIS DETAILS

1. 3D run

For the 3D run, the initial magnetic profile is

$$B_{L0}(N) = B_0 \left[(0.5 + S)^2 + 1 - \left(\frac{B_{M0}}{B_0} \right)^2 \right]^{1/2} \text{sgn}(N - N_n), \quad (\text{A1})$$

$$B_{M0}(N) = B_0 \left[\frac{1 - b_{Ms}}{2} \tanh\left(\frac{N - N_{TD}}{\lambda_{TD}}\right) + \frac{1 + b_{Ms}}{2} \right],$$

where $S = \tanh[(N - N_n)/\lambda]$. The primary reconnection current sheet is located at $N_n = 2.2d_i$, while the TD is initially located at $N_{TD} = -3.0d_i$. Parameter $b_{Ms} = \cos\phi - 0.5 \sin\phi$ determines the net rotational angle ϕ of the TD, and we used $\phi = 45^\circ$, as illustrated in Fig. 7(a), which was chosen based on the largest angular deflections observed upstream of the EDR in Fig. 2(b). The initial half-thicknesses of the current sheet and TD are $\lambda = 0.8d_i$ and $\lambda_{TD} = 1.3d_i$, respectively. These magnetic components are shown as dashed curves in Fig. 7(b).

The plasma has the same density profile $n = n_0[1 - (S + S^2)/3]$ as in Liu *et al.*, which is $n_2 = n_0/3$ and $n_1 = n_0$, where the subscripts “1” and “2” correspond to the magnetosheath and magnetosphere sides, respectively. The uniform total temperature is $T = 3B_0^2/(8\pi n_0)$ that consists of contributions from ions and electrons with ratio $T_i/T_e = 5$. The mass ratio is $m_i/m_e = 25$. The ratio of the electron plasma to gyro-frequency is $\omega_{pe}/\Omega_{ce} = 4$, where $\omega_{pe} \equiv (4\pi n_0 e^2/m_e)^{1/2}$ and $\Omega_{ce} \equiv eB_0/m_e c$. In the presentation, densities, time, velocities, spatial scales, magnetic fields, and electric fields are normalized to n_0 , the ion gyro-frequency Ω_{ci} , the Alfvénic speed $V_A \equiv B_0/(4\pi n_0 m_i)^{1/2}$, the ion inertia length $d_i \equiv c/\omega_{pi}$, B_0 and $V_A B_0/c$, respectively.

From Liu *et al.*, we determined the preferred orientation of the primary x-line of this asymmetric current sheet, which we align with the \mathbf{y} axis of our simulation. Thus, we rotate the simulation box by $\theta_{box} = -13^\circ$. The resulting magnetic field in the new coordinate will be

$$B_L(N) = B_{L0}(N) \cos\theta_{box} + B_{M0}(N) \sin\theta_{box}, \quad (\text{A2})$$

$$B_M(N) = -B_{L0}(N) \sin\theta_{box} + B_{M0}(N) \cos\theta_{box},$$

and they are shown as solid curves in Fig. 7(b). This large 3D run has a domain size $L_L \times L_M \times L_N = 300d_i \times 256d_i \times 28d_i$ and $4800 \times 4096 \times 448$ cells. The origin of the coordinate locates at the center of this simulation domain. This run has 0.88×10^{12} macro particles.

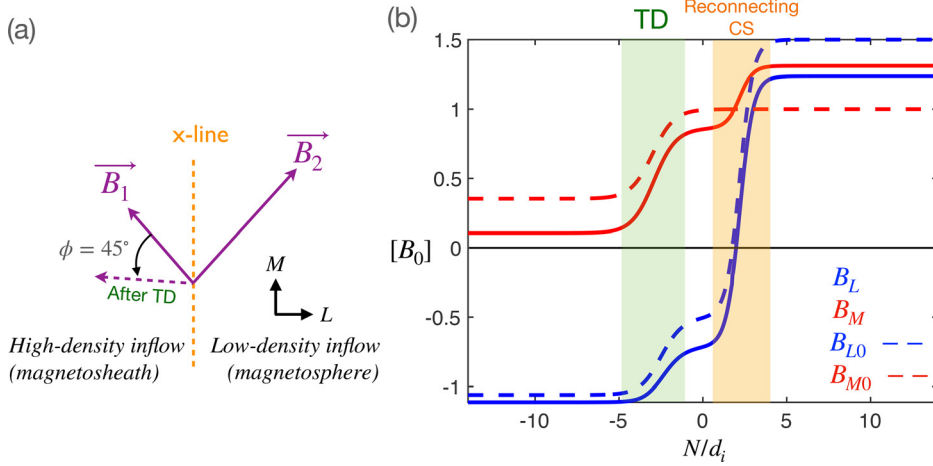


FIG. 7. Initial magnetic field condition used for the 3D PIC simulation. (a) Illustration of the magnetic field rotation in the TD on the magnetosheath side. (b) Initial profiles of B_L , B_M , B_{M0} , and B_{L0} .

The boundary conditions are periodic in both the L - and M -directions, while in the N -direction, they are conducting for fields and reflecting for particles. We use the perturbation to uniformly initiate a reconnection x-line along the M -direction at $L = 0$.

2. 2.5D run

The initial magnetic field profile of the 2.5D run is

$$\begin{aligned} B_{L0}(N) &= B_0(0.5 + S), \\ B_{M0}(N) &= B_0. \end{aligned} \tag{A3}$$

No upstream TD is present in the 2.5D run. The simulation domain size is $L_L \times L_N = 300d_i \times 28d_i$ or 4800×448 cells. The number of particles per species per cell is 400. All other parameters are set identically to the 3D run.

APPENDIX B: EFFECT OF THE NORMALIZED RECONNECTION RATE ASSUMPTION ON THE MULTI-EVENT STUDY

Here, we demonstrate that the exact choice of the normalized reconnection rate ($R = 0.2$) does not substantially affect the results of this study. To do so, we

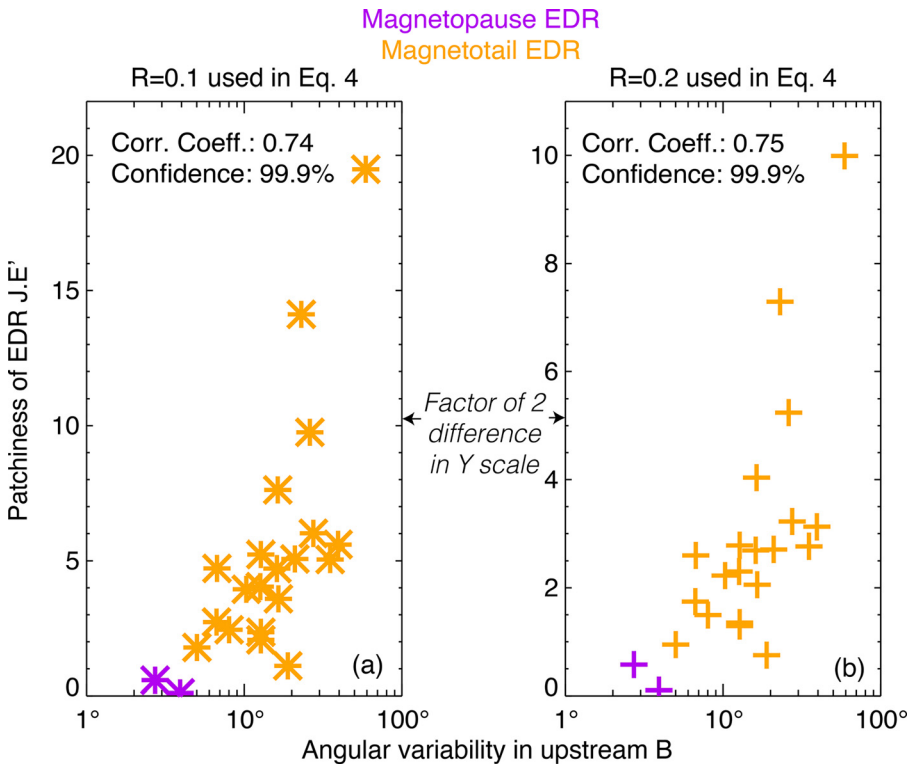


FIG. 8. Both (a) and (b) are laid out identically to Fig. 4(b). (a) The patchiness is evaluated using a normalized reconnection rate of $R = 0.1$. (b) The patchiness is evaluated identically to Fig. 4(b), e.g., using $R = 0.2$.

- reevaluate Eq. (4) for our 22 EDRs using $R = 0.1$,
- determine the strength and significance of the correlation between the patchiness of the EDR $\bar{J} \cdot \bar{E}$ and the angular variability of the upstream magnetic field, and
- compare with the results of Fig. 4(b), which was determined using $R = 0.2$.

Figure 8(a) shows results for $R = 0.1$, while Fig. 8(b) shows results for $R = 0.2$. The correlation coefficients are nearly identical (0.74 for $R = 0.1$ and 0.75 for $R = 0.2$), and both correlations are significant (99.9% confidence). There is roughly a factor of 2 difference between the patchiness parameters of Figs. 8(a) and 8(b), corresponding to the factor of 2 difference in R . Likely, this simple scaling with R is due to the fact that R appears in the normalization factor of Eq. (4), so increasing R by some decreases the patchiness by roughly the same factor. The main takeaway is that, for patchy events, the energy conversion rates are not controlled by a steady reconnection electric field with a normalized strength of order 0.1.

REFERENCES

- B. U. Ö. Sonnerup, "Magnetic field reconnection," in *Solar System Plasma Physics* (North-Holland Publishing Co., Amsterdam, 1979), Vol. 3, pp. 45–108.
- J. L. Burch and J. F. Drake, "Reconnecting magnetic fields: The huge amounts of energy released from the relinking of magnetic fields in outer space are both mysterious and potentially destructive," *Am. Sci.* **97**, 392–399 (2009).
- V. M. Vasyliunas, "Theoretical models of magnetic field line merging," *Rev. Geophys.* **13**, 303–336, <https://doi.org/10.1029/RG013i001p00303> (1975).
- M. Hesse, T. Neukirch, K. Schindler, M. Kuznetsova, and S. Zenitani, "The diffusion region in collisionless magnetic reconnection," *Space Sci. Rev.* **160**, 3–23 (2011).
- M. Hesse, Y. H. Liu, L. J. Chen, N. Bessho, S. Wang, J. L. Burch, T. Moretto, C. Norgren, K. J. Genestreti, T. D. Phan, and P. Tenfjord, "The physical foundation of the reconnection electric field," *Phys. Plasmas* **25**, 032901 (2018).
- J. L. Burch, T. E. Moore, R. B. Torbert, and B. L. Giles, "Magnetospheric Multiscale overview and science objectives," *Space Sci. Rev.* **199**, 5–21 (2016).
- R. B. Torbert, J. L. Burch, T. D. Phan, M. Hesse, M. R. Argall, J. Shuster, R. E. Ergun, L. Alm, R. Nakamura, K. J. Genestreti, D. J. Gershman, W. R. Paterson, D. L. Turner, I. Cohen, B. L. Giles, C. J. Pollock, S. Wang, L. J. Chen, J. E. Stawarz, J. P. Eastwood, K. J. Hwang, C. Farrugia, I. Dors, H. Vaith, C. Mouikis, A. Ardakani, B. H. Mauk, S. A. Fuselier, C. T. Russell, R. J. Strangeway, T. E. Moore, J. F. Drake, M. A. Shay, Y. V. Khotyaintsev, P. A. Lindqvist, W. Baumjohann, F. D. Wilder, N. Ahmadi, J. C. Dorelli, L. A. Avanov, M. Oka, D. N. Baker, J. F. Fennell, J. B. Blake, A. N. Jaynes, O. L. Contel, S. M. Petrinec, B. Lavraud, and Y. Saito, "Electron-scale dynamics of the diffusion region during symmetric magnetic reconnection in space," *Science* **362**, 1391–1395 (2018).
- K. J. Genestreti, T. K. M. Nakamura, R. Nakamura, R. E. Denton, R. B. Torbert, J. L. Burch, F. Plaschke, S. A. Fuselier, R. E. Ergun, B. L. Giles, and C. T. Russell, "How accurately can we measure the reconnection rate E_M for the MMS diffusion region event of 11 July 2017?," *J. Geophys. Res.: Space Phys.* **123**, 9130–9149, <https://doi.org/10.1029/2018JA025711> (2018).
- T. K. M. Nakamura, K. J. Genestreti, Y.-H. Liu, R. Nakamura, W.-L. Teh, H. Hasegawa, W. Daughton, M. Hesse, R. B. Torbert, J. L. Burch, and B. L. Giles, "Measurement of the magnetic reconnection rate in the Earth's magnetotail," *J. Geophys. Res.: Space Phys.* **123**, 9150–9168, <https://doi.org/10.1029/2018JA025713> (2018).
- N. Bessho, L.-J. Chen, S. Wang, and M. Hesse, "Effect of the reconnection electric field on electron distribution functions in the diffusion region of magnetotail reconnection," *Geophys. Res. Lett.* **45**, 12142–12152, <https://doi.org/10.1029/2018GL081216> (2018).
- J. L. Burch, R. B. Torbert, T. D. Phan, L.-J. Chen, T. E. Moore, R. E. Ergun, J. P. Eastwood, D. J. Gershman, P. A. Cassak, M. R. Argall, S. Wang, M. Hesse, C. J. Pollock, B. L. Giles, R. Nakamura, B. H. Mauk, S. A. Fuselier, C. T. Russell, R. J. Strangeway, J. F. Drake, M. A. Shay, Y. V. Khotyaintsev, P.-A. Lindqvist, G. Marklund, F. D. Wilder, D. T. Young, K. Torkar, J. Goldstein, J. C. Dorelli, L. A. Avanov, M. Oka, D. N. Baker, A. N. Jaynes, K. A. Goodrich, I. J. Cohen, D. L. Turner, J. F. Fennell, J. B. Blake, J. Clemmons, M. Goldman, D. Newman, S. M. Petrinec, K. J. Trattner, B. Lavraud, P. H. Reiff, W. Baumjohann, W. Magnes, M. Steller, W. Lewis, Y. Saito, V. Coffey, and M. Chandler, "Electron-scale measurements of magnetic reconnection in space," *Science* **352**, 1176 (2016).
- J. L. Burch, R. E. Ergun, P. A. Cassak, J. M. Webster, R. B. Torbert, B. L. Giles, J. C. Dorelli, A. C. Rager, K.-J. Hwang, T. D. Phan, K. J. Genestreti, R. C. Allen, L.-J. Chen, S. Wang, D. Gershman, O. L. Contel, C. T. Russell, R. J. Strangeway, F. D. Wilder, D. B. Graham, M. Hesse, J. F. Drake, M. Swisdak, L. M. Price, M. A. Shay, P.-A. Lindqvist, C. J. Pollock, R. E. Denton, and D. L. Newman, "Localized oscillatory energy conversion in magnetopause reconnection," *Geophys. Res. Lett.* **45**, 1237–1245, <https://doi.org/10.1002/2017GL076809> (2018).
- J. L. Burch, J. M. Webster, K. J. Genestreti, R. B. Torbert, B. L. Giles, S. A. Fuselier, J. C. Dorelli, A. C. Rager, T. D. Phan, R. C. Allen, L. J. Chen, S. Wang, O. L. Contel, C. T. Russell, R. J. Strangeway, R. E. Ergun, A. N. Jaynes, P. A. Lindqvist, D. B. Graham, F. D. Wilder, K. J. Hwang, and J. Goldstein, "Wave phenomena and beam-plasma interactions at the magnetopause reconnection region," *J. Geophys. Res.: Space Phys.* **123**, 1118–1133, <https://doi.org/10.1002/2017JA024789> (2018).
- J. L. Burch, J. M. Webster, M. Hesse, K. J. Genestreti, R. E. Denton, T. D. Phan, H. Hasegawa, P. A. Cassak, R. B. Torbert, B. L. Giles, D. J. Gershman, R. E. Ergun, C. T. Russell, R. J. Strangeway, O. L. Contel, K. R. Pritchard, A. T. Marshall, K.-J. Hwang, K. Dokgo, S. A. Fuselier, L.-J. Chen, S. Wang, M. Swisdak, J. F. Drake, M. R. Argall, K. J. Trattner, M. Yamada, and G. Paschmann, "Electron inflow velocities and reconnection rates at Earth's magnetopause and magnetosheath," *Geophys. Res. Lett.* **47**, e2020GL089082, <https://doi.org/10.1029/2020GL089082> (2020).
- P. A. Cassak, K. J. Genestreti, J. L. Burch, T.-D. Phan, M. A. Shay, M. Swisdak, J. F. Drake, L. Price, S. Eriksson, R. E. Ergun, B. J. Anderson, V. G. Merkin, and C. M. Komar, "The effect of a guide field on local energy conversion during asymmetric magnetic reconnection: Particle-in-cell simulations," *J. Geophys. Res.: Space Phys.* **122**, 11523–11542, <https://doi.org/10.1002/2017JA024555> (2017).
- K. J. Genestreti, J. L. Burch, P. A. Cassak, R. B. Torbert, R. E. Ergun, A. Varsani, T. D. Phan, B. L. Giles, C. T. Russell, S. Wang, M. Akhavan-Tafti, and R. C. Allen, "The effect of a guide field on local energy conversion during asymmetric magnetic reconnection: MMS observations," *J. Geophys. Res.: Space Phys.* **122**, 11342–11353, <https://doi.org/10.1002/2017JA024247> (2017).
- K. J. Genestreti, A. Varsani, J. L. Burch, P. A. Cassak, R. B. Torbert, R. Nakamura, R. E. Ergun, T.-D. Phan, S. Toledo-Redondo, M. Hesse, S. Wang, B. L. Giles, C. T. Russell, Z. Vörös, K.-J. Hwang, J. P. Eastwood, B. Lavraud, C. P. Escoubert, R. C. Fear, Y. Khotyaintsev, T. K. M. Nakamura, J. M. Webster, and W. Baumjohann, "Mms observation of asymmetric reconnection supported by 3-D electron pressure divergence," *J. Geophys. Res.: Space Phys.* **123**, 1806–1821, <https://doi.org/10.1002/2017JA025019> (2018).
- S. A. Fuselier, S. K. Vines, J. L. Burch, S. M. Petrinec, K. J. Trattner, P. A. Cassak, L.-J. Chen, R. E. Ergun, S. Eriksson, B. L. Giles, D. B. Graham, Y. V. Khotyaintsev, B. Lavraud, W. S. Lewis, J. Mukherjee, C. Norgren, T.-D. Phan, C. T. Russell, R. J. Strangeway, R. B. Torbert, and J. M. Webster, "Large-scale characteristics of reconnection diffusion regions and associated magnetopause crossings observed by MMS," *J. Geophys. Res.: Space Phys.* **122**, 5466–5486, <https://doi.org/10.1002/2017JA024024> (2017).
- J. P. Eastwood, T. D. Phan, M. Øieroset, and M. A. Shay, "Average properties of the magnetic reconnection ion diffusion region in the Earth's magnetotail: The 2001–2005 Cluster observations and comparison with simulations," *J. Geophys. Res.: Space Phys.* **115**, A08215, <https://doi.org/10.1029/2009JA014962> (2010).
- P. A. Cassak and M. A. Shay, "Scaling of asymmetric magnetic reconnection: General theory and collisional simulations," *Phys. Plasmas* **14**, 102114 (2007).
- P. A. Cassak and M. A. Shay, "Scaling of asymmetric Hall magnetic reconnection," *Geophys. Res. Lett.* **35**, L19102, <https://doi.org/10.1029/2008GL035268> (2008).
- P. L. Pritchett and F. S. Mozer, "The magnetic field reconnection site and dissipation region," *Phys. Plasmas* **16**, 080702 (2009).
- M. Swisdak, J. F. Drake, L. Price, J. L. Burch, P. A. Cassak, and T.-D. Phan, "Localized and intense energy conversion in the diffusion region of asymmetric

- magnetic reconnection," *Geophys. Res. Lett.* **45**, 5260–5267, <https://doi.org/10.1029/2017GL076862> (2018).
- ²⁴K. R. Pritchard, J. L. Burch, S. A. Fuselier, J. M. Webster, R. B. Torbert, M. R. Argall, J. Broll, K. J. Genestreti, B. L. Giles, O. L. Contel, J. Mukherjee, T. D. Phan, A. C. Rager, C. T. Russell, and R. J. Strangeway, "Energy conversion and electron acceleration in the magnetopause reconnection diffusion region," *Geophys. Res. Lett.* **46**, 10274–10282, <https://doi.org/10.1029/2019GL084636> (2019).
- ²⁵M. Swisdak, B. N. Rogers, J. F. Drake, and M. A. Shay, "Diamagnetic suppression of component magnetic reconnection at the magnetopause," *J. Geophys. Res.: Space Phys.* **108**, 1218, <https://doi.org/10.1029/2002JA009726> (2003).
- ²⁶L. Price, M. Swisdak, J. F. Drake, P. A. Cassak, J. T. Dahlin, and R. E. Ergun, "The effects of turbulence on three-dimensional magnetic reconnection at the magnetopause," *Geophys. Res. Lett.* **43**, 6020–6027, <https://doi.org/10.1002/2016GL069578> (2016).
- ²⁷R. E. Ergun, L.-J. Chen, F. D. Wilder, N. Ahmadi, S. Eriksson, M. E. Usanova, K. A. Goodrich, J. C. Holmes, A. P. Sturmer, D. M. Malaspina, D. L. Newman, R. B. Torbert, M. R. Argall, P.-A. Lindqvist, J. L. Burch, J. M. Webster, J. F. Drake, L. Price, P. A. Cassak, M. Swisdak, M. A. Shay, D. B. Graham, R. J. Strangeway, C. T. Russell, B. L. Giles, J. C. Dorelli, D. Gershman, L. Avano, M. Hesse, B. Lavraud, O. L. Contel, A. Retino, T. D. Phan, M. V. Goldman, J. E. Stawarz, S. J. Schwartz, J. P. Eastwood, K.-J. Hwang, R. Nakamura, and S. Wang, "Drift waves, intense parallel electric fields, and turbulence associated with asymmetric magnetic reconnection at the magnetopause," *Geophys. Res. Lett.* **44**, 2978–2986 (2017).
- ²⁸R. E. Ergun, S. Hoilijoki, N. Ahmadi, S. J. Schwartz, F. D. Wilder, J. L. Burch, R. B. Torbert, P.-A. Lindqvist, D. B. Graham, R. J. Strangeway, O. L. Contel, J. C. Holmes, J. E. Stawarz, K. A. Goodrich, S. Eriksson, B. L. Giles, D. Gershman, and L. J. Chen, "Magnetic reconnection in three dimensions: Observations of electromagnetic drift waves in the adjacent current sheet," *J. Geophys. Res.: Space Phys.* **124**, 10104, <https://doi.org/10.1029/2019JA027228> (2019).
- ²⁹R. E. Ergun, S. Hoilijoki, N. Ahmadi, S. J. Schwartz, F. D. Wilder, J. F. Drake, M. Hesse, M. A. Shay, H. Ji, M. Yamada, D. B. Graham, P. A. Cassak, M. Swisdak, J. L. Burch, R. B. Torbert, J. C. Holmes, J. E. Stawarz, K. A. Goodrich, S. Eriksson, R. J. Strangeway, and O. LeContel, "Magnetic reconnection in three dimensions: Modeling and analysis of electromagnetic drift waves in the adjacent current sheet," *J. Geophys. Res.: Space Phys.* **124**, 10085, <https://doi.org/10.1029/2019JA027275> (2019).
- ³⁰D. B. Graham, Y. V. Khotyaintsev, C. Norgren, A. Vaivads, M. André, S. Toledo-Redondo, P.-A. Lindqvist, G. T. Marklund, R. E. Ergun, W. R. Paterson, D. J. Gershman, B. L. Giles, C. J. Pollock, J. C. Dorelli, L. A. Avano, B. Lavraud, Y. Saito, W. Magnes, C. T. Russell, R. J. Strangeway, R. B. Torbert, and J. L. Burch, "Lower hybrid waves in the ion diffusion and magnetospheric inflow regions," *J. Geophys. Res.: Space Phys.* **122**, 517–533, <https://doi.org/10.1002/2016JA023572> (2017).
- ³¹A. Le, W. Daughton, L.-J. Chen, and J. Egedal, "Enhanced electron mixing and heating in 3-D asymmetric reconnection at the earth's magnetopause," *Geophys. Res. Lett.* **44**, 2096–2104, <https://doi.org/10.1002/2017GL072522> (2017).
- ³²F. D. Wilder, R. E. Ergun, S. Hoilijoki, J. Webster, M. R. Argall, N. Ahmadi, S. Eriksson, J. L. Burch, R. B. Torbert, O. L. Contel, R. J. Strangeway, and B. L. Giles, "A survey of plasma waves appearing near dayside magnetopause electron diffusion region events," *J. Geophys. Res.: Space Phys.* **124**, 7837–7849, <https://doi.org/10.1029/2019JA027060> (2019).
- ³³M. Hesse, N. Aunai, D. Sibeck, and J. Birn, "On the electron diffusion region in planar, asymmetric systems," *Geophys. Res. Lett.* **41**, 8673–8680, <https://doi.org/10.1002/2014GL061586> (2014).
- ³⁴F. D. Wilder, R. E. Ergun, S. Eriksson, T. D. Phan, J. L. Burch, N. Ahmadi, K. A. Goodrich, D. L. Newman, K. J. Trattner, R. B. Torbert, B. L. Giles, R. J. Strangeway, W. Magnes, P.-A. Lindqvist, and Y.-V. Khotyaintsev, "Multipoint measurements of the electron jet of symmetric magnetic reconnection with a moderate guide field," *Phys. Rev. Lett.* **118**, 265101 (2017).
- ³⁵S. Eriksson, F. D. Wilder, R. E. Ergun, S. J. Schwartz, P. A. Cassak, J. L. Burch, L.-J. Chen, R. B. Torbert, T. D. Phan, B. Lavraud, K. A. Goodrich, J. C. Holmes, J. E. Stawarz, A. P. Sturmer, D. M. Malaspina, M. E. Usanova, K. J. Trattner, R. J. Strangeway, C. T. Russell, C. J. Pollock, B. L. Giles, M. Hesse, P.-A. Lindqvist, J. F. Drake, M. A. Shay, R. Nakamura, and G. T. Marklund, "Magnetospheric Multiscale observations of the electron diffusion region of large guide field magnetic reconnection," *Phys. Rev. Lett.* **117**, 015001 (2016).
- ³⁶J. L. Burch and T. D. Phan, "Magnetic reconnection at the dayside magnetopause: Advances with MMS," *Geophys. Res. Lett.* **43**, 8327–8338, <https://doi.org/10.1002/2016GL069787> (2016).
- ³⁷J. Burch, K. Dokgo, K. Hwang, R. Torbert, D. Graham, J. Webster, R. Ergun, B. Giles, R. Allen, L.-J. Chen, S. Wang, K. Genestreti, C. Russell, R. Strangeway, and O. L. Contel, "High-frequency wave generation in magnetotail reconnection: Linear dispersion analysis," *Geophys. Res. Lett.* **46**, 4089–4097, <https://doi.org/10.1029/2019GL082471> (2019).
- ³⁸K. Dokgo, K.-J. Hwang, J. L. Burch, E. Choi, P. H. Yoon, D. G. Sibeck, and D. B. Graham, "High-frequency wave generation in magnetotail reconnection: Nonlinear harmonics of upper hybrid waves," *Geophys. Res. Lett.* **46**, 7873–7882, <https://doi.org/10.1029/2019GL083361> (2019).
- ³⁹Y. V. Khotyaintsev, D. B. Graham, K. Steinva, L. Alm, A. Vaivads, A. Johlander, C. Norgren, W. Li, A. Divin, H. S. Fu, K.-J. Hwang, J. L. Burch, N. Ahmadi, O. L. Contel, D. J. Gershman, C. T. Russell, and R. B. Torbert, "Electron heating by Debye-scale turbulence in guide-field reconnection," *Phys. Rev. Lett.* **124**, 045101 (2020).
- ⁴⁰J. D. Huba, N. T. Gladd, and J. F. Drake, "The lower hybrid drift instability in nonantiparallel reversed field plasmas," *J. Geophys. Res.: Space Phys.* **87**, 1697–1701, <https://doi.org/10.1029/JA087iA03p01697> (1982).
- ⁴¹L. Price, M. Swisdak, J. F. Drake, and D. B. Graham, "Turbulence and transport during guide field reconnection at the magnetopause," *J. Geophys. Res.: Space Phys.* **125**, e2019JA027498, <https://doi.org/10.1029/JA087iA03p01697> (2020).
- ⁴²M. Hesse, N. Aunai, S. Zenitani, M. Kuznetsova, and J. Birn, "Aspects of collisionless magnetic reconnection in asymmetric systems," *Phys. Plasmas* **20**, 061210 (2013).
- ⁴³Y.-H. Liu, M. Hesse, T. C. Li, M. Kuznetsova, and A. Le, "Orientation and stability of asymmetric magnetic reconnection x line," *J. Geophys. Res.: Space Phys.* **123**, 4908–4920, <https://doi.org/10.1029/2018JA025410> (2018).
- ⁴⁴T. K. M. Nakamura, H. Hasegawa, K. J. Genestreti, R. E. Denton, T. D. Phan, J. E. Stawarz, R. Nakamura, and W. D. Nystrom, "Fast cross-scale energy transfer during turbulent magnetic reconnection," *Geophys. Res. Lett.* **48**, e2021GL093524, <https://doi.org/10.1029/2021GL093524> (2021).
- ⁴⁵S. F. Spinnangr, P. Tenfjord, M. Hesse, C. Norgren, H. M. Kolsto, N. K. Kwagala, T. M. Jørgensen, and J. Pérez-Coll Jiménez, "Asymmetrically varying guide field during magnetic reconnection: Particle-in-cell simulations," *J. Geophys. Res.: Space Phys.* **127**, e021JA029955, <https://doi.org/10.1029/2021JA029955> (2021).
- ⁴⁶W. Daughton, V. Roytershteyn, H. Karimabadi, L. Yin, B. J. Albright, B. Bergen, and K. J. Bowers, "Role of electron physics in the development of turbulent magnetic reconnection in collisionless plasmas," *Nat. Phys.* **7**, 539–542 (2011).
- ⁴⁷G. Lapenta, S. Markidis, M. V. Goldman, and D. L. Newman, "Secondary reconnection sites in reconnection-generated flux ropes and reconnection fronts," *Nat. Phys.* **11**, 690–695 (2015).
- ⁴⁸R. E. Ergun, K. A. Goodrich, F. D. Wilder, J. C. Holmes, J. E. Stawarz, S. Eriksson, A. P. Sturmer, D. M. Malaspina, M. E. Usanova, R. B. Torbert, P. A. Lindqvist, Y. Khotyaintsev, J. L. Burch, R. J. Strangeway, C. T. Russell, C. J. Pollock, B. L. Giles, M. Hesse, L. J. Chen, G. Lapenta, M. V. Goldman, D. L. Newman, S. J. Schwartz, J. P. Eastwood, T. D. Phan, F. S. Mozer, J. Drake, M. A. Shay, P. A. Cassak, R. Nakamura, and G. Marklund, "Magnetospheric Multiscale satellites observations of parallel electric fields associated with magnetic reconnection," *Phys. Rev. Lett.* **116**, 235102 (2016).
- ⁴⁹Y.-H. Liu, M. Hesse, F. Guo, W. Daughton, H. Li, P. A. Cassak, and M. A. Shay, "Why does steady-state magnetic reconnection have a maximum local rate of order 0.1?," *Phys. Rev. Lett.* **118**, 085101 (2017).
- ⁵⁰Y.-H. Liu, M. Hesse, P. A. Cassak, M. A. Shay, S. Wang, and L. J. Chen, "On the collisionless asymmetric magnetic reconnection rate," *Geophys. Res. Lett.* **45**, 3311–3318, <https://doi.org/10.1002/2017GL076460> (2018).
- ⁵¹R. B. Torbert, J. L. Burch, M. R. Argall, L. Alm, C. J. Farrugia, T. G. Forbes, B. L. Giles, A. Rager, J. Dorelli, R. J. Strangeway, R. E. Ergun, F. D. Wilder, N. Ahmadi, P. A. Lindqvist, and Y. Khotyaintsev, "Structure and dissipation characteristics of an electron diffusion region observed by MMS during a rapid,

- normal-incidence magnetopause crossing,” *J. Geophys. Res.: Space Phys.* **122**, 11901–11916, <https://doi.org/10.1002/2017JA024579> (2017).
- ⁵²S. A. Fuselier, W. S. Lewis, C. Schiff, R. Ergun, J. L. Burch, S. M. Petrinec, and K. J. Trattner, “Magnetospheric Multiscale Science mission profile and operations,” *Space Sci. Rev.* **199**, 77–103 (2016).
- ⁵³C. Pollock, T. Moore, A. Jacques, J. Burch, U. Gliese, Y. Saito, T. Omoto, L. Avanov, A. Barrie, V. Coffey, J. Dorelli, D. Gershman, B. Giles, T. Rosnack, C. Salo, S. Yokota, M. Adrian, C. Aoustin, C. Auletta, S. Aung, V. Bigio, N. Cao, M. Chandler, D. Chornay, K. Christian, G. Clark, G. Collinson, T. Corris, A. De Los Santos, R. Devlin, T. Diaz, T. Dickerson, C. Dickson, A. Diekmann, F. Diggs, C. Duncan, A. Figueroa-Vinas, C. Firman, M. Freeman, N. Galassi, K. Garcia, G. Goodhart, D. Guerrero, J. Hageman, J. Hanley, E. Hemminger, M. Holland, M. Hutchins, T. James, W. Jones, S. Kreisler, J. Kujawski, V. Lavu, J. Lobell, E. LeCompte, A. Lukemire, E. MacDonald, A. Mariano, T. Mukai, K. Narayanan, Q. Nguyen, M. Onizuka, W. Paterson, S. Persyn, B. Piepgrass, F. Cheney, A. Rager, T. Raghuram, A. Ramil, L. Reichenthal, H. Rodriguez, J. Rouzaud, A. Rucker, Y. Saito, M. Samara, J.-A. Sauvaud, D. Schuster, M. Shappirio, K. Shelton, D. Sher, D. Smith, K. Smith, S. Smith, D. Steinfeld, R. Szymkiewicz, K. Tanimoto, J. Taylor, C. Tucker, K. Tull, A. Uhl, J. Vloet, P. Walpole, S. Weidner, D. White, G. Winkert, P.-S. Yeh, and M. Zeuch, “Fast plasma investigation for Magnetospheric Multiscale,” *Space Sci. Rev.* **199**, 331–406 (2016).
- ⁵⁴D. T. Young, J. L. Burch, R. G. Gomez, A. De Los Santos, G. P. Miller, P. Wilson, N. Paschalidis, S. A. Fuselier, K. Pickens, E. Hertzberg, C. J. Pollock, J. Scherrer, P. B. Wood, E. T. Donald, D. Aaron, J. Furman, D. George, R. S. Gurnee, R. S. Hourani, A. Jacques, T. Johnson, T. Orr, K. S. Pan, S. Persyn, S. Pope, J. Roberts, M. R. Stokes, K. J. Trattner, and J. M. Webster, “Hot plasma composition analyzer for the Magnetospheric Multiscale Mission,” *Space Sci. Rev.* **199**, 407–470 (2016).
- ⁵⁵P.-A. Lindqvist, G. Olsson, R. B. Torbert, B. King, M. Granoff, D. Rau, G. Needell, S. Turco, I. Dors, P. Beckman, J. Macri, C. Frost, J. Salwen, A. Eriksson, L. Åhlén, Y. V. Khotyaintsev, J. Porter, K. Lappalainen, R. E. Ergun, W. Wermeier, and S. Tucker, “The spin-plane double probe electric field instrument for MMS,” *Space Sci. Rev.* **199**, 137–165 (2016).
- ⁵⁶R. E. Ergun, S. Tucker, J. Westfall, K. A. Goodrich, D. M. Malaspina, D. Summers, J. Wallace, M. Karlsson, J. Mack, N. Brennan, B. Pyke, P. Withnell, R. Torbert, J. Macri, D. Rau, I. Dors, J. Needell, P.-A. Lindqvist, G. Olsson, and C. M. Cully, “The axial double probe and fields signal processing for the MMS mission,” *Space Sci. Rev.* **199**, 167–188 (2016).
- ⁵⁷C. T. Russell, B. J. Anderson, W. Baumjohann, K. R. Bromund, D. Dearborn, D. Fischer, G. Le, H. K. Leinweber, D. Leneman, W. Magnes, J. D. Means, M. B. Moldwin, R. Nakamura, D. Pierce, F. Plaschke, K. M. Rowe, J. A. Slavin, R. J. Strangeway, R. Torbert, C. Hagen, I. Jernej, A. Valavanoglou, and I. Richter, “The Magnetospheric Multiscale Magnetometers,” *Space Sci. Rev.* **199**, 189–256 (2016).
- ⁵⁸T. D. Phan, J. P. Eastwood, P. A. Cassak, M. Øieroset, J. T. Gosling, D. J. Gershman, F. S. Mozer, M. A. Shay, M. Fujimoto, W. Daughton, J. F. Drake, J. L. Burch, R. B. Torbert, R. E. Ergun, L. J. Chen, S. Wang, C. Pollock, J. C. Dorelli, B. Lavraud, B. L. Giles, T. E. Moore, Y. Saito, L. A. Avanov, W. Paterson, R. J. Strangeway, C. T. Russell, Y. Khotyaintsev, P. A. Lindqvist, M. Oka, and F. D. Wilder, “MMS observations of electron-scale filamentary currents in the reconnection exhaust and near the X line,” *Geophys. Res. Lett.* **43**, 6060–6069, <https://doi.org/10.1002/2016GL069212> (2016).
- ⁵⁹T. D. Phan, J. F. Drake, M. A. Shay, F. S. Mozer, and J. P. Eastwood, “Evidence for an elongated (>60 ion skin depths) electron diffusion region during fast magnetic reconnection,” *Phys. Rev. Lett.* **99**, 255002 (2007).
- ⁶⁰L.-J. Chen, N. Bessho, B. Lefebvre, H. Vaith, A. Fazakerley, A. Bhattacharjee, P. A. Puhl-Quinn, A. Runov, Y. Khotyaintsev, A. Vaivads, E. Georgescu, and R. Torbert, “Evidence of an extended electron current sheet and its neighboring magnetic island during magnetotail reconnection,” *J. Geophys. Res.: Space Phys.* **113**, A12213, <https://doi.org/10.1029/2008JA013385> (2008).
- ⁶¹S. Zenitani, M. Hesse, A. Klimas, and M. Kuznetsova, “New measure of the dissipation region in collisionless magnetic reconnection,” *Phys. Rev. Lett.* **106**, 195003 (2011).
- ⁶²R. Wang, Q. Lu, S. Lu, C. T. Russell, J. L. Burch, D. J. Gershman, W. Gonzalez, and S. Wang, “Physical implication of two types of reconnection electron diffusion regions with and without ion-coupling in the magnetotail current sheet,” *Geophys. Res. Lett.* **47**, e2020GL088761, <https://doi.org/10.1029/2020GL088761> (2020).
- ⁶³D. S. Payne, C. J. Farrugia, R. B. Torbert, K. Germaschewski, A. R. Rogers, and M. R. Argall, “Origin and structure of electromagnetic generator regions at the edge of the electron diffusion region,” *Phys. Plasmas* **28**, 112901 (2021).
- ⁶⁴L.-J. Chen, M. Hesse, S. Wang, D. Gershman, R. Ergun, C. Pollock, R. Torbert, N. Bessho, W. Daughton, J. Dorelli, B. Giles, R. Strangeway, C. Russell, Y. Khotyaintsev, J. Burch, T. Moore, B. Lavraud, T. Phan, and L. Avanov, “Electron energization and mixing observed by MMS in the vicinity of an electron diffusion region during magnetopause reconnection,” *Geophys. Res. Lett.* **43**, 6036–6043, <https://doi.org/10.1002/2016GL069215> (2016).
- ⁶⁵L. J. Chen, M. Hesse, S. Wang, D. Gershman, R. E. Ergun, J. Burch, N. Bessho, R. B. Torbert, B. Giles, J. Webster, C. Pollock, J. Dorelli, T. Moore, W. Paterson, B. Lavraud, R. Strangeway, C. Russell, Y. Khotyaintsev, P. A. Lindqvist, and L. Avanov, “Electron diffusion region during magnetopause reconnection with an intermediate guide field: Magnetospheric Multiscale observations,” *J. Geophys. Res.: Space Phys.* **122**, 5235–5246, <https://doi.org/10.1002/2017JA024004> (2017).
- ⁶⁶B. Lavraud, Y. C. Zhang, Y. Vernisse, D. J. Gershman, J. Dorelli, P. A. Cassak, J. Dargent, C. Pollock, B. Giles, N. Aunai, M. Argall, L. Avanov, A. Barrie, J. Burch, M. Chandler, L.-J. Chen, G. Clark, I. Cohen, V. Coffey, J. P. Eastwood, J. Egedal, S. Eriksson, R. Ergun, C. J. Farrugia, S. A. Fuselier, V. Génot, D. Graham, E. Grigorenko, H. Hasegawa, C. Jacquey, I. Kacem, Y. Khotyaintsev, E. MacDonald, W. Magnes, A. Marchaudon, B. Mauk, T. E. Moore, T. Mukai, R. Nakamura, W. Paterson, E. Penou, T. D. Phan, A. Rager, A. Retino, Z. J. Rong, C. T. Russell, Y. Saito, J.-A. Sauvaud, S. J. Schwartz, C. Shen, S. Smith, R. Strangeway, S. Toledo-Redondo, R. Torbert, D. L. Turner, S. Wang, and S. Yokota, “Currents and associated electron scattering and bouncing near the diffusion region at Earth’s magnetopause,” *Geophys. Res. Lett.* **43**, 3042–3050, <https://doi.org/10.1002/2016GL068359> (2016).
- ⁶⁷J. M. Webster, J. L. Burch, P. H. Reiff, A. G. Daou, K. J. Genestreti, D. B. Graham, R. B. Torbert, R. E. Ergun, S. Y. Sazykin, A. Marshall, R. C. Allen, L.-J. Chen, S. Wang, T. D. Phan, B. L. Giles, T. E. Moore, S. A. Fuselier, G. Cozzani, C. T. Russell, S. Eriksson, A. C. Rager, J. M. Broll, K. Goodrich, and F. Wilder, “Magnetospheric Multiscale dayside reconnection electron diffusion region events,” *J. Geophys. Res.: Space Phys.* **123**, 4858–4878, <https://doi.org/10.1029/2018JA025245> (2018).
- ⁶⁸W. Y. Li, D. B. Graham, Y. V. Khotyaintsev, A. Vaivads, M. André, K. Min, K. Liu, B. B. Tang, C. Wang, K. Fujimoto, C. Norgren, S. Toledo-Redondo, P. A. Lindqvist, R. E. Ergun, R. B. Torbert, A. C. Rager, J. C. Dorelli, D. J. Gershman, B. L. Giles, B. Lavraud, F. Plaschke, W. Magnes, O. Le Contel, C. T. Russell, and J. L. Burch, “Electron Bernstein waves driven by electron currents near the electron diffusion region,” *Nat. Commun.* **11**, 141 (2020).
- ⁶⁹M. Zhou, X. H. Deng, Z. H. Zhong, Y. Pang, R. X. Tang, M. El-Alaoui, R. J. Walker, C. T. Russell, G. Lapenta, R. J. Strangeway, R. B. Torbert, J. L. Burch, W. R. Paterson, B. L. Giles, Y. V. Khotyaintsev, R. E. Ergun, and P. A. Lindqvist, “Observations of an electron diffusion region in symmetric reconnection with weak guide field,” *Astrophys. J.* **870**, 34 (2019).
- ⁷⁰R. E. Denton, B. U. Ö. Sonnerup, C. T. Russell, H. Hasegawa, T. D. Phan, R. J. Strangeway, B. L. Giles, R. E. Ergun, P. A. Lindqvist, R. B. Torbert, J. L. Burch, and S. K. Vines, “Determining *L-M-N* current sheet coordinates at the magnetopause from Magnetospheric Multiscale data,” *J. Geophys. Res.: Space Phys.* **123**, 2274–2295, <https://doi.org/10.1002/2017JA024619> (2018).
- ⁷¹Q. Q. Shi, C. Shen, Z. Y. Pu, M. W. Dunlop, Q. G. Zong, H. Zhang, C. J. Xiao, Z. X. Liu, and A. Balogh, “Dimensional analysis of observed structures using multipoint magnetic field measurements: Application to cluster,” *Geophys. Res. Lett.* **32**, L12105, <https://doi.org/10.1029/2005GL022454> (2005).
- ⁷²G. Paschmann, I. Papamastorakis, W. Baumjohann, N. Scoppe, C. W. Carlson, B. U. Ö. Sonnerup, and H. Lühr, “The magnetopause for large magnetic shear: AMPTE/IRM observations,” *J. Geophys. Res.* **91**, 11099–11115, <https://doi.org/10.1029/JA091iA10p11099> (1986).
- ⁷³B. U. Ö. Sonnerup, “On the stress balance in flux transfer events,” *J. Geophys. Res.* **92**, 8613–8620, <https://doi.org/10.1029/JA092iA08p08613> (1987).
- ⁷⁴B. U. Ö. Sonnerup and L. J. Cahill, Jr., “Magnetopause structure and attitude from explorer 12 observations,” *J. Geophys. Res.* **72**, 171, <https://doi.org/10.1029/JZ072i001p00171> (1967).

- ⁷⁵J. L. Myers, A. D. Well, and R. F. Lorch, Jr., *Research Design and Statistical Analysis* (Routledge, 2013).
- ⁷⁶K. J. Bowers, B. J. Albright, L. Yin, B. Bergen, and T. J. T. Kwan, “Ultra-high performance three-dimensional electromagnetic relativistic kinetic plasma simulations,” *Phys. Plasmas* **15**, 055703 (2008).
- ⁷⁷R. Nakamura, K. J. Genestreti, T. Nakamura, W. Baumjohann, A. Varsani, T. Nagai, N. Bessho, J. L. Burch, R. E. Denton, J. P. Eastwood, R. E. Ergun, D. J. Gershman, B. L. Giles, H. Hasegawa, M. Hesse, P.-A. Lindqvist, C. T. Russell, J. E. Stawarz, R. J. Strangeway, and R. B. Torbert, “Structure of the current sheet in the 11 July 2017 electron diffusion region event,” *J. Geophys. Res.: Space Phys.* **124**, 1173–1186, <https://doi.org/10.1029/2018JA026028> (2019).
- ⁷⁸H. Man, M. Zhou, Z. Zhong, and X. Deng, “Intense energy conversion events at the magnetopause boundary layer,” *Geophys. Res. Lett.* **49**, e2022GL098069, <https://doi.org/10.1029/2022GL098069> (2022).
- ⁷⁹S. A. Fuselier, J. M. Webster, K. J. Trattner, S. M. Petriner, K. J. Genestreti, K. R. Pritchard, K. Llera, J. M. Broll, J. L. Burch, and R. J. Strangeway, “Reconnection X-line orientations at the Earth’s magnetopause,” *J. Geophys. Res.: Space Phys.* **126**, e2021JA029789, <https://doi.org/10.1029/2021JA029789> (2021).
- ⁸⁰V. Angelopoulos, P. Cruce, A. Drozdov, E. W. Grimes, N. Hatzigeorgiu, D. A. King, D. Larson, J. W. Lewis, J. M. McTiernan, D. A. Roberts, C. L. Russell, T. Hori, Y. Kasahara, A. Kumamoto, A. Matsuoka, Y. Miyashita, Y. Miyoshi, I. Shinohara, M. Teramoto, J. B. Faden, A. J. Halford, M. McCarthy, R. M. Millan, J. G. Sample, D. M. Smith, L. A. Woodger, A. Masson, A. A. Narock, K. Asamura, T. F. Chang, C. Y. Chiang, Y. Kazama, K. Keika, S. Matsuda, T. Segawa, K. Seki, M. Shoji, S. W. Y. Tam, N. Umemura, B. J. Wang, S. Y. Wang, R. Redmon, J. V. Rodriguez, H. J. Singer, J. Vandegriff, S. Abe, M. Nose, A. Shinbori, Y. M. Tanaka, S. UeNo, L. Andersson, P. Dunn, C. Fowler, J. S. Halekas, T. Hara, Y. Harada, C. O. Lee, R. Lillis, D. L. Mitchell, M. R. Argall, K. Bromund, J. L. Burch, I. J. Cohen, M. Galloy, B. Giles, A. N. Jaynes, O. Le Contel, M. Oka, T. D. Phan, B. M. Walsh, J. Westlake, F. D. Wilder, S. D. Bale, R. Livi, M. Pulupa, P. Whittlesey, A. DeWolfe, B. Harter, E. Lucas, U. Auster, J. W. Bonnell, C. M. Cully, E. Donovan, R. E. Ergun, H. U. Frey, B. Jackel, A. Keiling, H. Korth, J. P. McFadden, Y. Nishimura, F. Plaschke, P. Robert, D. L. Turner, J. M. Weygand, R. M. Candey, R. C. Johnson, T. Kovalick, M. H. Liu, R. E. McGuire, A. Breneman, K. Kersten, and P. Schroeder, “The space physics environment data analysis system (SPEDAS),” *Space Sci. Rev.* **215**, 9 (2019).
- ⁸¹MMS Team, see <https://lasp.colorado.edu/mms/sdc/public/> for “MMS Science Data Center” (2015–present).